

UC Irvine

UC Irvine Previously Published Works

Title

Structural and Chemical Properties of Gold Rare Earth Disilicide Core–Shell Nanowires

Permalink

<https://escholarship.org/uc/item/0ss583fm>

Journal

ACS Nano, 5(1)

ISSN

1936-0851

Authors

Ouyang, Wenjie

Shinde, Aniketa

Zhang, Yanning

et al.

Publication Date

2011-01-25

DOI

10.1021/nn102230j

Copyright Information

This work is made available under the terms of a Creative Commons Attribution License, available at <https://creativecommons.org/licenses/by/4.0/>

Peer reviewed

Structural and Chemical Properties of Gold Rare Earth Disilicide Core–Shell Nanowires

Wenjie Ouyang,^{†,*} Aniketa Shinde,^{†,§} Yanning Zhang,[†] Juxian Cao,[†] Regina Ragan,[§] and Ruqian Wu^{†,**}

[†]Department of Electronic Information, Wuhan University, Wuhan 430072, People's Republic of China, [‡]Department of Physics and Astronomy, University of California, Irvine, California 92697-4575, United States, and [§]Department of Chemical Engineering and Materials Science, University of California, Irvine, California 92697-2575, United States

To make significant progress in the development of innovative nanotechnologies, it is crucial to not only fabricate nanomaterials but also understand the origins of their new physical properties. Strong quantum confinement effects and high surface/bulk ratios exhibited in nanometer-scale structures often yield interesting features that are extremely useful in broad applications, from catalysis to nanophotonics. For the rational development of nanosystems, it is desired to find correlations among different physical and chemical properties that are governed by a few key factors. For instance, Norskov *et al.* found from theoretical calculations that activities of metallic and bimetallic surfaces can be correlated well to the shift of their d-band centers.¹ It was also shown that catalytic reaction rates, in the context of electrochemical catalysis, exhibit an exponential dependence on the catalyst work function.² The establishment of these connections and the clear understanding of the underlying physical mechanism will undoubtedly levitate the effectiveness of the search of new nanocatalysts.

Here we investigate an experimental core–shell metallic system, Au on dysprosium disilicide nanowires, and compare theoretically predicted changes in electronic structure with experimental observations. Rare earth disilicide (RESi₂) nanowires, since first observed to self-assemble on silicon substrates,^{3,4} have attracted extensive attention in the past decade as they have low Schottky barriers on the n-type Si.^{5,6} Various RESi₂^{7,8} and YSi₂⁹ nanowires grown on flat or vicinal Si(001) surfaces have been found to exhibit tunable quantum confinement effects, and furthermore, they permit fabrication and manipulation of metallic

ABSTRACT Clear understanding of the relationship between electronic structure and chemical activity will aid in the rational design of nanocatalysts. Core–shell Au-coated dysprosium and yttrium disilicide nanowires provide a model atomic scale system to understand how charges that transfer across interfaces affect other electronic properties and in turn surface activities toward adsorbates. Scanning tunneling microscopy data demonstrate self-organized growth of Au-coated DySi₂ nanowires with a nanometer feature size on Si(001), and Kelvin probe force microscopy data measure a reduction of work function that is explained in terms of charge transfer. Density functional theory calculations predict the preferential adsorption site and segregation path of Au adatoms on Si(001) and YSi₂. The chemical properties of Au–YSi₂ nanowires are then discussed in light of charge density, density of states, and adsorption energy of CO molecules.

KEYWORDS: density functional calculation · scanning tunneling microscopy · Kelvin probe force microscopy · CO oxidation · Au core–shell nanowire

and bimetallic nanostructures by coating them with Au, Pd, or Pt.¹⁰ Although RESi₂ nanowires are highly active and tend to decompose in ambient conditions, Pt-coated RESi₂ nanowires have been found to be rather stable even under reactive ion-etching conditions.^{11,12} Several advantages of these nanosystems, *e.g.*, their uniform and controllable size and shape and negligible diffusion of metal atoms to the interior region, and resistance against thermal coalescence are very attractive for making novel nanocatalysts.

To further develop these nanosystems for practical applications, synergistic density functional calculations and scanning probe microscopy (SPM) studies are performed in this work. Au nanoclusters have been found to display unusually high activity toward catalyzing various chemical reactions, such as CO oxidation, when their size is reduced to 2–3 nm.^{13–16} To our knowledge, the catalytic activity of Au/disilicide nanostructures has not been measured yet. Due to the change of support and morphology, the chemical properties of Au/disilicide

*Address correspondence to wur@uci.edu.

Received for review August 31, 2010 and accepted December 07, 2010.

Published online December 13, 2010. 10.1021/nn102230j

© 2011 American Chemical Society

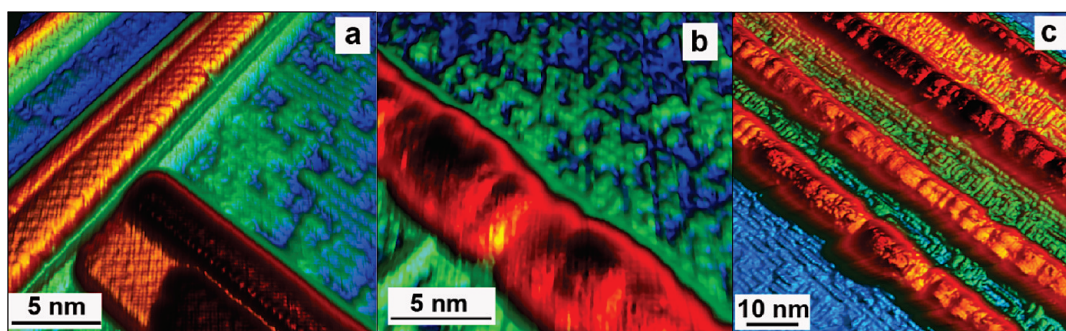


Figure 1. STM images of DySi₂ nanowires: (a) before Au deposition obtained with $V_{\text{bias}} = -1.6$ V and 200 pA tunneling current, (b) after Au deposition obtained with $V_{\text{bias}} = -1.8$ V and 200 pA tunneling current, and (c) a different sample after Au deposition obtained with $V_{\text{bias}} = -1.95$ V and 100 pA tunneling current. Warm to cold colors reflect high to low surface corrugations.

nanostructures might be substantially different from other Au nanosystems that have been explored extensively in the last two decades. It is therefore essential to establish their structural models and furthermore to probe their electronic structures and surface activities toward small adsorbates. Using SPM data and *ab initio* results, we provide an understanding of the kinetics and the energetics leading to formation of Au/RESi₂ nanostructures. The establishment of atomic models for the Au–disilicide systems allows further investigations of their electronic and chemical properties. Interestingly, we found that charge transfer from Au adatoms to the nanowires simultaneously determines energy position of Au d-orbitals, surface work function, and, moreover, CO adsorption energy. Simple relationships between different physical quantities offer useful insights for understanding of these new core–shell metallic nanostructures.

RESULTS AND DISCUSSION

Au Aggregation on Disilicide Nanowire Surfaces. Scanning tunneling microscopy (STM) images of DySi₂ nanowires on the p-type Si(001) surface before and after Au deposition are shown in Figure 1a and b, respectively. In Figure 1a, we show that the DySi₂ nanowire surface before Au deposition exhibits a $c(2 \times 2)$ reconstruction, as was also observed by others for DySi₂¹⁷ and ErSi₂¹⁸ nanostructures. Meanwhile, the neighboring regions comprise both (2×1) reconstructed Si(001) surface manifested by Si dimer rows and complex Dy–Si metal reconstructed regions. Figure 1b shows a DySi₂ nanowire/Si(001) surface after Au deposition and annealing at 550 °C. The DySi₂ nanowire surface no longer exhibits the $c(2 \times 2)$ reconstruction that is seen in Figure 1a but instead has a corrugated surface that is indicative of Au aggregation on the surface. The neighboring Si(001) surface again shows a combination of Si dimer rows and metal reconstructed regions. Another DySi₂ nanowire/Si(001) sample was prepared, and a STM image after Au deposition is shown in Figure 1c. In this sample, corrugations are also evident on the nanowire surfaces, and Si dimer rows are observed on the neigh-

boring substrate area. Since we observed Au clusters forming on DySi₂ nanowire surfaces but not on the Si(001) substrate at lower Au coverage, this indicates a preferential aggregation of Au on the nanowire surface versus Si(001). It appears that Au clusters will form on Si(001) if the Au coverage exceeds the nanowire surface density. This is clearly demonstrated in the Supporting Information where STM images of DySi₂ before Au (Figure S1a), after Au deposition for 1 min (Figure S1b), and after Au deposition for 2 min (Figure S1c) are given. These results show that the thickness of Au on DySi₂ is within the monolayer range.

In order to understand the mechanism of the preferential Au aggregation on the nanowire surfaces exhibited in the STM results, we performed first principles calculations of Au adsorption on the YSi₂ nanowire and the Si(001) surface. We used a double-layer $3a_{\text{Si}}$ -wide YSi₂ nanowire on Si(001) as the template for studies of the energetics of Au aggregation. The double-layer $3a_{\text{Si}}$ -wide YSi₂ nanowire structure has been determined to be a stable minimum-energy structure and is consistent with experimental observations of multilayer growth,^{17,19} also evident in the STM image of Figure 1a. The double-layer $3a_{\text{Si}}$ -wide YSi₂ surface has two Si dimer rows on top, separated by a trench over the central Y atoms. The top- and side-views of the optimized surface model are shown in Figure 2a and b, that consists of one double layer $3a_{\text{Si}}$ -wide YSi₂ nanowire on a 6-layer Si slab. A monolayer of hydrogen atoms was incorporated to passivate the dangling bonds at the bottom surface of the slab. To mimic Au adsorption on an isolated nanowire, we used a (1×8) supercell in the lateral plane. The positions of H atoms and three bottom layers of Si atoms were fixed while all the other atoms were allowed to relax, with a criterion that the calculated force on each atom is smaller than 0.01 eV/Å. Convergence tests were performed to optimize number of k -points, thickness of slab, and energy cutoff. The $5 \times 1 \times 1$ k -points were found sufficient to sample the essentially one-dimensional Brillouin zone.

To identify stable adsorption geometries for systems with N_{Au} gold atoms in the unit cell, we calculate

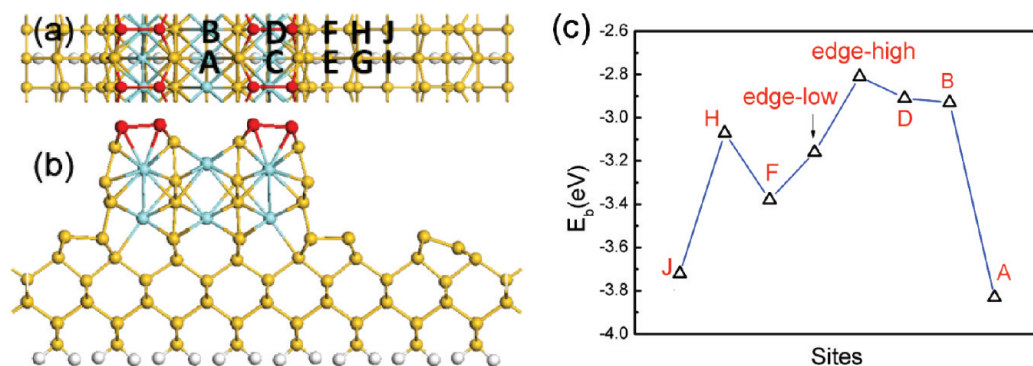


Figure 2. The (a) top- and (b) side-views of the relaxed ball-and-stick model for the YSi₂/Si system. The cyan, white, and yellow spheres represent Y, H, and Si atoms, respectively. Surface Si dimers in nanowire are colored in red. (c) Adsorption energies of Au on sites along a segregation path J → H → F → edge-low → edge-high → D → B → A.

and compare the site dependent adsorption energies defined as

$$E_b = (E_t - N_{Au}E_{Au} - E_s)/N_{Au} \quad (1)$$

Here, E_t is the total energy of Au/YSi₂/Si(001), E_{Au} is the energy per Au atom, and E_s is the total energy of the YSi₂/Si(001) template. First, total energies were calculated for a single Au adatom on the eight nonequivalent high-symmetry adsorption sites highlighted in Figure 2a for quantitative comparison of the site preference. In order to calculate the adsorption energies associated with these sites, the vertical position of the Au adatom was allowed to relax on sites A–D and G–J, while the lateral coordinates of Au were fixed. However, lateral positions of the Au adatom on sites E and F were also allowed to relax, since binding sites near the edge of the nanowire are not clearly defined.

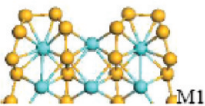

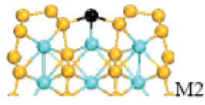
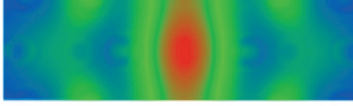
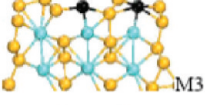

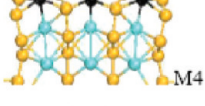
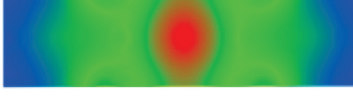
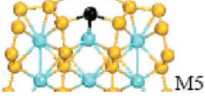

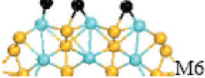

From the calculated total energies, we identified a segregation path of the Au adatom along a direction that is perpendicular to the nanowire, and the values of E_b for Au at different adsorption sites are given in Figure 2c. The most stable adsorption site for the Au adatom is on site A over the nanowire surface, with an adsorption energy of $E_{b,A} = -3.83$ eV. This is much lower than corresponding values for Au at adjacent site B ($E_{b,B} = -2.93$ eV), C ($E_{b,C} = -3.06$ eV), and D ($E_{b,D} = -2.91$ eV), indicating that site A is very attractive for the Au adatom once it is on top of the YSi₂ nanowire. Similarly, the open site J serves as the attractive center on Si(001) since the adsorption energy there ($E_{b,J} = -3.72$ eV) is also much lower than those of Au at surrounding sites: G ($E_{b,G} = -3.15$ eV), H ($E_{b,H} = -3.07$ eV), and I ($E_{b,I} = -2.38$ eV). In fact, the Au adatom directly migrated to site E ($E_{b,E} = -3.26$ eV) or J from their initial positions on site G or I when lateral motion was allowed in the structural optimization procedure.

It is interesting to note that $E_{b,A}$ is 0.11 eV lower than $E_{b,J}$, which suggests that for Au to bind at site A is about 20 times more preferable than to bind at site J at room temperature, according to a simple estimate using Boltzmann statistics. Therefore, Au adatoms tend to diffuse toward nanowires in ambient conditions, in

good accordance with our experimental findings. Along the path from site J to A: J → H → F → edge-low → edge-high → D → B → A, the activation energy for Au migration is ~1.0 eV, indicating a high probability of diffusion of Au toward the nanowire under our experimental condition, $T = 550$ °C. The steepest changes in energy along this path occur at J → H and B → A, with an energy cost or gain of 0.65 and 0.9 eV, respectively. Au adatoms appear to be rather mobile in other regions, even to climb up the wire. We found that Au induces large reconstruction in the YSi₂ nanowire and the Si(001) surface. For example, the Si dimer rows on top of the YSi₂ nanowire, highlighted by red balls in Figure 2a and b, are pushed apart by more than 1 Å with the presence of the Au adatom at site A.

We then performed calculations for cases with two and three Au adatoms on YSi₂ nanowires, for comparison to our experiments. From extensive tests with different initial geometries, we identified several preferential geometries and list them in Table 1. The most stable geometry for two Au adatoms on the nanowire is shown as model-3 (M3) in which Au adatoms take the A and C sites. This structure has an adsorption energy of -3.50 eV per adatom, slightly better than the average of $E_{b,A}$ and $E_{b,C}$ for single Au, -3.45 eV, benefiting from the Au–Au interaction. However, the best configuration for two Au is to have them taking the A and J sites; the adsorption energy for this configuration is the same as the average of $E_{b,A}$ and $E_{b,J}$, 3.78 eV, since they are well separated in space (~12 Å apart). The third Au adatom, essentially making monolayer coverage over the nanowire, takes the other C site (*cf.* M4 in Table 1). The adsorption energy for this structure is around -3.39 eV per adatoms, still better than the average adsorption energies of three individual Au adatoms: $(E_{b,A} + 2E_{b,C})/3 = -3.32$ eV. Another possible model is where Au forms a cluster (actually a wire) along the trough of YSi₂ nanowires (M5), but its adsorption energy is slightly higher than that of M4. Interestingly, we noted that Au adatoms in M4 cause significant expansion of Si dimers on the YSi₂ nanowire. If we remove the capping Si and directly place Au on Y as depicted in model M6, then

TABLE 1. Side Views of the Relaxed Structural Models for $\text{YSi}_2/\text{Si}(001)$ and $\text{Au}/\text{YSi}_2/\text{Si}(001)$ ^a

| Structure | E_{b} | $E_{\text{b,CO}}$ | Work function (eV)* |
|--|----------------|-------------------|--|
|  M1 | | |  |
|  M2 | -3.83 | -0.52 |  |
|  M3 | -3.50 | -0.52 |  |
|  M4 | -3.39 | -0.23 |  |
|  M5 | -3.31 | -0.51 |  |
|  M6 | -3.90 | -0.46 |  |

^aCyan, yellow, and black spheres represent Y, Si, and Au atoms, respectively. E_{b} and $E_{\text{b,CO}}$ are adsorption energies (in eV) of Au on $\text{YSi}_2/\text{Si}(001)$ and CO on $\text{Au}/\text{YSi}_2/\text{Si}(001)$, respectively. A red-to-blue color band was used to show the calculated work functions in a horizontal plane 2.8 \AA over $\text{YSi}_2/\text{Si}(001)$ and $\text{Au}/\text{YSi}_2/\text{Si}(001)$ in a range of 4.3 (red) to 4.9 eV (blue).

the adsorption energy may approach a value as high as -3.90 eV .²⁰ From M2–M4 to M6, one may find that the presence of Au adatoms on top of the disilicide nanowire surfaces substantially distorts and finally destabilizes Si bonds. As discussed below, this stems from the substantial charge transfer from Au adatoms to their surrounding regions, which weakens the Si–Si bonds by filling the antibonding states of Si.

From the adsorption energies, we may conclude that most Au adatoms tend to aggregate to nanowires if the Au coverage matches the nanowire surface density, to form structures like M6 and M4. Moreover, we found that the adsorption energies for two and three Au adatoms around site J are 0.27 and 0.31 eV less favored compared to M3 and M4, respectively. Note that

the presence of Au only causes a minimal change in the nanowire height, a fact that is also confirmed by the experimental data. In the Supporting Information, we show the line profiles across DySi_2 nanowires in Figure S2. The average nanowire heights before and after Au deposition are approximately 0.95 and 1.00 nm, respectively.

Electronic Structure of Au/Disilicide Nanowires. Since the adsorption energies of single Au adatom on sites A and J are much lower than those on other sites, we first examine the local charge densities of these two configurations in order to understand the site preference of Au on $\text{YSi}_2/\text{Si}(001)$ versus on $\text{Si}(001)$. Charge density differences, $\Delta\rho = \rho_{\text{Au}/\text{YSi}_2/\text{Si}(001)} - \rho_{\text{Au}} - \rho_{\text{YSi}_2/\text{Si}(001)}$, are shown in Figure 3 for Au at sites A and J. From contours of $\Delta\rho$ in

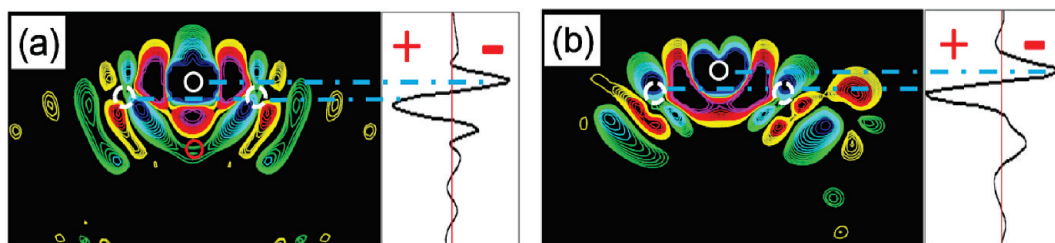


Figure 3. Charge density differences of (a) $\text{Au}/\text{YSi}_2/\text{Si}(001)$ and (b) $\text{Au}/\text{Si}(001)$. White solid circles represent the positions of Au; dashed circles represent the positions of Si atoms; and the red circle represents the position of Y atom. Cold colors (green, cyan, and blue) and warm colors (yellow, red, and pink) represent electron depletion and accumulation, respectively. Contours start from $\pm 1 \times 10^{-3} \text{ e}/\text{\AA}^3$ and change successively by a factor of 1.15. Line profiles on the side show the planar averages of the corresponding charge density differences along the vertical axis. Positive and negative signs represent the increase and decrease of electron density, respectively.

a cross-sectional plane passing through the Au adatom (highlighted by white circles), we found that electrons deplete from Au and accumulate in regions between Au and surrounding Si and Y atoms for both geometries in Figure 3a and b. This differs from the intuitive picture that Au gains electrons from Si because of its higher electronegativity. In Figure 3a, one may find that electrons accumulate between Au and two nearby Si atoms in the horizontal plane as well as between Au and Y in the vertical plane. This suggests the formation of Au–Si and Au–Y bonds in Au/YSi₂/Si(001). In Figure 3b, electrons also accumulate between Au and neighboring Si atoms in the horizontal plane, and the Au–Si bonds appear to be even stronger (larger pink area) for Au on the site J. However, this structure lacks the vertical Au–Y bond and thus is slightly less favorable than that of Au on the site A.

An important effect of the charge redistribution in Figure 3 is the apparent electron charge polarization from Au toward the substrate. To better appreciate this, we also give the planar average of $\Delta\rho$ as a line profile along the vertical direction on the right side of the corresponding contour plots of Figure 3. The outstanding feature in the $\Delta\rho(z)$ curves is that electrons transfer from the top-half of Au (signified by the negative sign) to the area under it (signified by the positive sign). This type of electron redistribution and polarization was also found in models with two and three Au adatoms shown in Table 1, except in M5 where the Au cluster draws electrons from Si. With electron accumulation at the bottom of Au nuclei, the presence of Au adatoms establishes an upward dipole layer on Si and YSi₂ nanowire surfaces. This reduces the average local potential around Au atoms and hence leads to decreases of the local work function and eigen energies of Au states.

The two-dimensional maps of the work function distribution on top of YSi₂/Si(001) and Au/YSi₂/Si(001) are plotted on the right column of Table 1, over a 15 Å wide region across the nanowire. The calculated local work functions are 4.9 eV over Si(001) and 4.6–4.9 eV over YSi₂/Si(001). The work function on top of Au/YSi₂/Si(001) is substantially reduced, especially if examined right above Au adatoms. Overall, calculations show that the presence of Au adatoms leads to a reduction of work function by 0.2–0.7 eV on the nanowire surface, with the largest reduction observed in M4. The exception is for M5, in which the formation of Au clusters actually enhances the local work function to >4.9 eV. This value is close to that of the clean Au(111) surface, 5.1–5.5 eV, as measured from Kelvin probe force microscopy (KPFM) and photoelectric effect measurements.²¹ We found that work function above the Au adatom on the Si(001) terrace is ~4.6 eV, also reduced by 0.3 eV from that of the clean Si(001) surface. Interestingly, work function varies over different Au adatoms in configurations M3, M4, and M6, owing to the dissimilar Au–Si and Au–Y bonds. For M3 and M4, the change of work

function is much more obvious over the Au adatom at the center than that of over the Au adatom at site C.

In order to experimentally probe how the work function evolves as Au is deposited on disilicide nanowire surfaces, simultaneous atomic force microscopy (AFM) topography and KPFM contact potential difference (CPD) data for DySi₂ nanowires were acquired before and after Au deposition. Figure 4a and b is 500 × 500 nm topography and CPD images, respectively, of a Dy/Si(001) sample before Au deposition. Figure 4c and d is topography and CPD images, respectively, of the same Dy/Si(001) sample after Au deposition. The color scales on the right of Figure 4b and d represent the work function of the surface. The method for determining the work function from KPFM-CPD data is discussed in the Supporting Information. By visual comparison of Figure 4b and d, it is clear that the work function decreases due to the presence of Au on the surface as predicted in the calculations shown in Table 1.

For quantitative evaluation, Table 2 lists the average work function values with standard deviation for two different samples of DySi₂ nanowires on Si(001) before and after Au deposition. The first data column gives the work function of the clean 2 × 1 reconstructed Si(001) surface from KPFM measurements. The p-type Si(001) substrate has a work function, 4.8–5.0 eV, in agreement with the theoretical value discussed above and also with the accepted value, 4.9 eV²² for the p-type Si at the dopant density listed by the manufacturer. It is obvious that work function values of Si(001) depend sensitively on the presence of metal adatoms on the surface. The second and third data columns in Table 2 provide the average work functions over regions on Si(001) between DySi₂ nanowires, as shown in Figure 4b and d, before and after Au deposition, respectively. The substrate work function decreases due to the presence of Dy and Au adatoms Si(001), indicating that the aggregation of both elements to nanowires is preferential but not selective. The accepted work function of DySi₂ thin films is 4.42 eV.³ The local work function of DySi₂ nanowires from CPD measurements is approximately 4.25 eV; it is reduced from the thin film value due to quantum size effect.⁸ KPFM measurements of Au on DySi₂ nanowires yield work functions between 3.9–4.0 eV, which is further reduced from the value of the nanowire work function. These experimental values are somewhat smaller than the calculated work functions displayed in Table 1, probably due to the difference in height of planes. Yet the Au-induced reduction of the work function agrees reasonably well between theory and experiment. For example, we measured a reduction in work function of ~0.35 eV on Si(001) and ~0.30 eV on YSi₂ nanowires due to Au deposition that correlates very well with DFT calculations. Since experimental results indicate no increase of work function after the deposition of Au, M5 is unlikely to form in real samples.

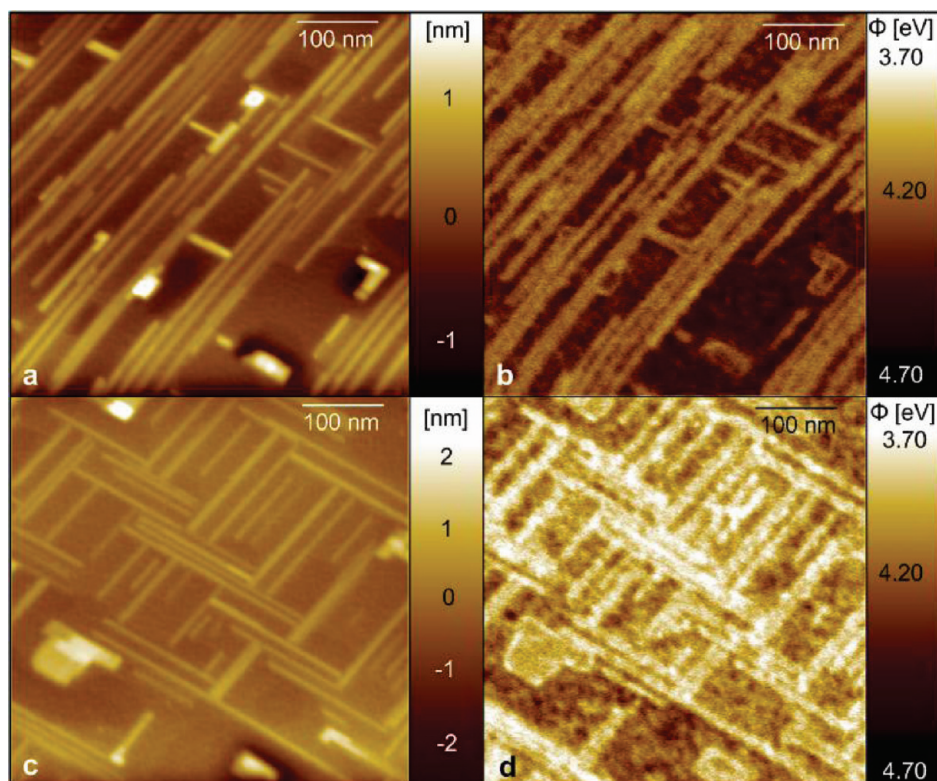


Figure 4. The 500×500 nm AFM topography (left) and KPFM (right) images for DySi_2 on $\text{Si}(001)$ before (a and b) and after (c and d) Au deposition. The color scale on the right displays the calculated work function from CPD data.

CO Adsorption on Au/YSi₂/Si(001). The varying properties of Au–disilicide systems in different geometries allow us to examine how adsorption energy of simple molecules correlates with electronic features, such as work functions. As mentioned before, both the Au d-band center and the local work function stem from the charge redistribution around Au adatoms. The former is known to be a key factor for the activity of metallic systems toward adsorptions and reactions of simple molecules such as CO.²³ Here we also use CO as the probing molecule and calculate the CO adsorption energy over different Au atoms as

$$E_{\text{b,CO}} = E_{\text{CO/Au/YSi}_2/\text{Si}(001)} - E_{\text{Au/YSi}_2/\text{Si}(001)} - E_{\text{CO}} \quad (2)$$

Here, total energies of Au/YSi₂/Si(001) ($E_{\text{Au/YSi}_2/\text{Si}(001)}$) and free CO molecule (E_{CO}) are used as the references. As depicted in Figure 5a, CO takes a straight adsorption geometry on a single Au adatom over YSi₂/Si(001). The equilibrium C–O bond length is 1.15 Å, and the C–Au bond length is 2.12 Å. The calculated value of $E_{\text{b,CO}}$ on Au/YSi₂/Si(001) is -0.52 eV. In fact, the CO adsorption energies are also around 0.5 eV on several configura-

tions of Au/YSi₂/Si(001) with more Au adatoms except M4. Note that systems with CO adsorption energies about -0.5 eV are appropriate for the purpose of catalyzing various reactions, in particular those with CO poisoning problems, as in fuel cells.²⁴ For Au/YSi₂/Si(001) with two or three Au adatoms, more than one site is available with varying CO adsorption energies. For example, CO adsorption energy in the configuration M6 changes from -0.19 and -0.42 to -0.46 eV on Au₁–Au₃, respectively, as denoted in Figure 5b. The availability of multiple attractive sites in a small area may find important use to catalyze chemical reactions, since they can optimally break chemical bonds of different reactants and provide the appropriate ensemble effect, as found on bimetallic surfaces.²⁵ Experimental and theoretical studies in this direction will be pursued in the future.

We also explore if there is a simple correlation between work function and CO adsorption energy of Au/YSi₂/Si(001). From the calculated values of $E_{\text{b,CO}}$ and Φ in Table 1, one may find that the correlation between $E_{\text{b,CO}}$ and the average work function of Au/YSi₂/Si(001) indeed exists if results for M5 are excluded. For ex-

TABLE 2. KPFM measured work functions for Au/Dy/p-type Si(001)

| | Si (001) Substrate Φ [eV] | | | DySi ₂ Nanowire Φ [eV] | |
|----------|--------------------------------|-----------------|-----------------|--|-----------------|
| | 2×1 reconstructed | after Dy dep | after Au dep | before Au dep | after Au dep |
| Sample 1 | 5.01 ± 0.06 | 4.54 ± 0.06 | 4.11 ± 0.06 | 4.21 ± 0.07 | 3.91 ± 0.07 |
| Sample 2 | 4.79 ± 0.08 | 4.51 ± 0.06 | 4.24 ± 0.07 | 4.29 ± 0.06 | 3.99 ± 0.07 |

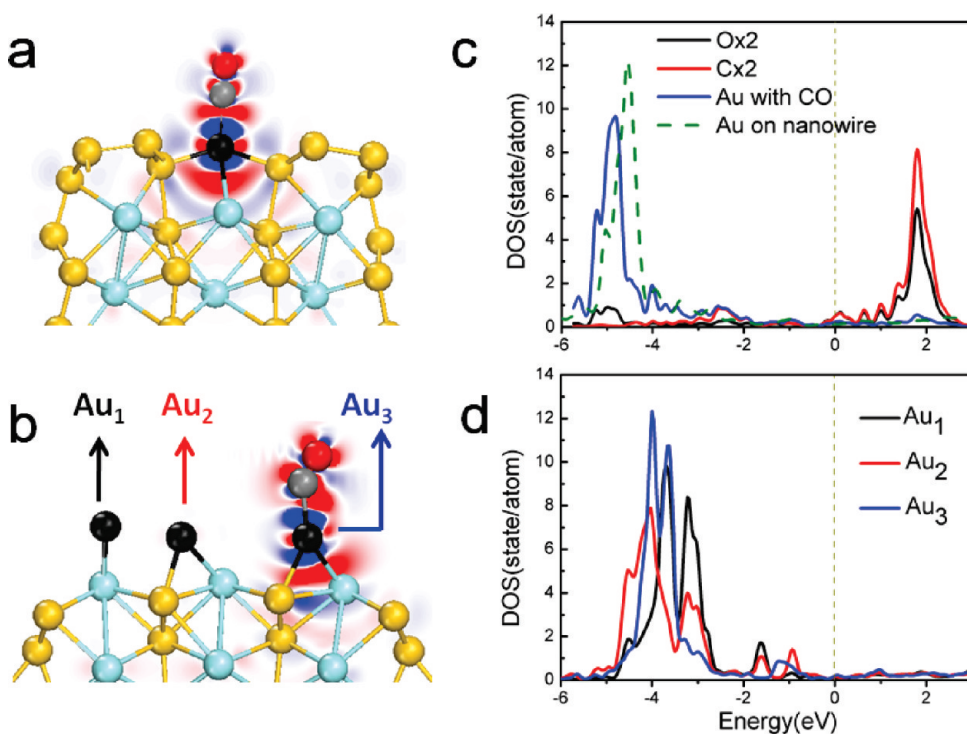


Figure 5. The relaxed atomic geometries and charge density differences of CO adsorption on Au/YSi₂/Si(001) in geometries of M2 and M6 denoted in Table 1 are found in (a and b). Red, gray, black, cyan, and yellow balls represent O, C, Au, Y, and Si atoms, respectively. The red contours represent areas of electron accumulation, whereas the blue contours represent electron depletion. The plots of density of states projected in different atoms are found in (c and d). The vertical line at zero is the position of the Fermi level.

ample, the M4 structure has the lowest $E_{b,CO}$ as well as the smallest work function among all models given in Table 1. The work function of M3 is higher than that of M2 at the center of the nanowire, but M3 has one additional Au aside, so the chemical activities of these two structures toward CO are similar. The projected density of states (PDOS) curves of Au adatoms plotted in Figure 5c and d indicate that Au d-band centers are typically low, as a result of the charge transfer from Au to the nanowire underneath. For instance, the top of Au d-band in the single Au/YSi₂/Si(001) shifts to 4 eV below the Fermi level in Figure 5c. In the structure M4, which has the smallest $E_{b,CO}$, the top of Au d-band is at $-4.5 \sim -4.8$ eV. Therefore, it appears that the CO adsorption energy, position of the d-band center, and local work function correlate well with each other in most of these systems.

The charge density differences in Figure 5a and b for CO on Au/YSi₂/Si(001) with either one or three Au adatoms suggest that the Au- e_g state donates electrons to the CO $2\pi^*$ orbitals. Bader charge analysis provides more information regarding the electron transfers on individual atoms.²⁶ For instance, CO gains 0.083 electron charge (0.076 e on C and 0.007 e on O) from Au/YSi₂/Si(001) (0.055 e from Au). We can see that the values of PDOS of Au around the Fermi level are very small in Figure 5c and d. Yet the CO $2\pi^*$ orbitals expand to a very wide range, with the tail extending to below the

Fermi level. The CO 5σ -orbital is also broadened to a small resonance peak at -2.5 eV in the PDOS plot in Figure 5c. It is interesting to note that the adsorption of CO causes additional charge accumulation under Au in Figure 5a and b. Obviously, chemical interaction between CO and Au/YSi₂/Si(001) is appreciable, in terms of adsorption energy, orbital hybridization, and charge transfer.

CONCLUSIONS

The preferential aggregation of Au on disilicide nanowire surfaces *versus* the Si(001) surface observed in STM experiments was found to be associated with a lower adsorption energy on nanowire surfaces *versus* Si(001). DFT calculations also revealed a diffusion path for Au adatoms on Si(001) and YSi₂ surfaces. The corresponding energy barrier, ~ 1.0 eV along this path, indicates that Au adatoms are mobile under growth conditions. This is the first study of the kinetics of aggregation of Au toward disilicide nanowire surfaces. Both KPFM measurements and DFT calculations indicate that the adsorption of Au reduces the local work function of disilicide nanowires and Si(001) surfaces. This change in work function could have implications in the chemical activity of Au on these surfaces. The resultant chemical properties of Au/YSi₂/Si(001) were probed and discussed in the context of CO adsorption. The CO adsorption energy indeed depends on the local work function for most cases; and the effect of different charge

transfer between Au and substrate was assigned as the origin. Thus this work provides a foundation for us-

ing charge transfer and work function to further understand chemical activity in nanosystems.

MATERIALS AND METHODS

All samples for our experimental observations were fabricated in an ultrahigh vacuum chamber with a base pressure of 8×10^{-11} Torr. The chamber is equipped with an Omicron variable temperature scanning probe microscopy (VT-SPM) system and an external Omicron Kelvin probe force microscope (KPFM) electronics module for *in situ* characterization. Silicon substrates were B-doped, with a resistivity in the range of 0.01–0.04 Ω -cm. Clean Si(001) (2×1) reconstructed surfaces were prepared using the standard protocols. Dy (99.9%, ESPI) was evaporated from a molybdenum crucible using a mini e-beam evaporator (Quad-EV-C, Mantis) at an emission power of approximately 20–23 W for 1 min to obtain a submonolayer coverage. During Dy deposition, the Si(001) substrates were held at 600 °C, and the chamber pressure was approximately 3×10^{-9} Torr. After Dy deposition, samples were postannealed at 630 °C for 2 min for the formation of DySi₂ nanostructures; these samples were subsequently analyzed with STM, AFM, and KPFM after returning to room temperature. After SPM characterization of DySi₂ nanostructures, Au was evaporated from a Au foil (0.1 mm thick, purity >99.999%, Alfa Aesar) on a vitreous carbon crucible at a power of 10 W for 1 min, and the sample was annealed post growth for 30 s at a substrate temperature of 550 °C for both instances. STM, AFM, and KPFM analyses were performed after the samples returned to room temperature. Details of our KPFM experimental setup can be found in ref 8.

First principles calculations were performed within the framework of DFT using the Vienna *ab initio* simulation package (VASP).²⁷ The generalized gradient approximation (GGA)²⁸ was used for the description of the exchange–correlation interaction among electrons. The projector augmented wave (PAW)²⁹ pseudopotentials were used to represent the ionic cores. We set an energy cutoff of 350 eV for the plane-wave basis expansion. To avoid complexity in dealing with the *f*-electrons of Dy, we used Y as a substitute throughout our calculations. Bulk YSi₂ has an identical crystal structure of hexagonal RE₂Si₂, and their lattice constants are also similar. Many previous publications have demonstrated the appropriateness of using Y as a RE substitute for theoretical studies of atomic geometries and chemical properties of these systems.^{30–32} The adsorption patterns of Y on Si(001)^{33,34} and the morphology of YSi₂ nanowires on Si(001) have been analyzed recently using DFT calculations and SPM measurements. In particular, DFT predicted that YSi₂ nanowires with a width of $3a_{\text{Si}}$ are the thinnest stable configuration on Si(001), in agreement with experimental observations for both YSi₂ and RE₂Si₂ nanowires.

Acknowledgment. This work was supported by the National Science Foundation (grant no. CBET-0731349) and Department of Energy (grant no. DE-FG02-05ER46237). Calculations were performed on supercomputers of National Energy Research Scientific Computing Center.

Supporting Information Available: Principles of Kelvin probe force microscopy and calibration of tip work function are described. Table S1: Contact potential difference data from DySi₂ nanoisland calibration sample and tip work function calculated from the known work function of the calibration sample. Figure S1: Scanning tunneling microscopy images of DySi₂ nanowires on Si(001) (a) before Au deposition, (b) after Au deposition for 1 min and (c) after Au deposition for 2 min acquired at with $V_{\text{bias}} = -1.9$ V and 100 pA tunneling current. Figure S2: Line profiles obtained across nanowires before and after Au deposition as shown in Figure (a) S1a and (b) S1b, respectively. This material is available free of charge via the Internet at <http://pubs.acs.org>.

REFERENCES AND NOTES

1. Hammer, B.; Morikawa, Y.; Nørskov, J. K. CO Chemisorption at Metal Surfaces and Overlayers. *Phys. Rev. Lett.* **1996**, *76*, 2141–2144.
2. Bebelis, S.; Vayenas, C. G. Non-Faradaic Electrochemical Modification of Catalytic Activity: 1. The Case of Ethylene Oxidation on Pt. *J. Catal.* **1989**, *118*, 125–146.
3. Preinesberger, C.; Vandr , S.; Kalka, T.; D hne-Prietsch, M. Formation of Dysprosium Silicide Wires on Si(001). *J. Phys. D: Appl. Phys.* **1998**, *31*, L43–L45.
4. Chen, Y.; Ohlberg, D. A. A.; Medeiros-Ribeiro, G.; Chang, Y. A.; Williams, R. S. Self-Assembled Growth of Epitaxial Erbium Disilicide Nanowires on Silicon (001). *Appl. Phys. Lett.* **2002**, *76*, 4004–4006.
5. Tu, K. N.; Thompson, R. D.; Tsaur, B. Y. Contact Reaction between Si and Rare Earth Metals. *Appl. Phys. Lett.* **1981**, *38*, 535–537.
6. Owen, J. H. G.; Miki, K.; Bowler, D. R. Self-Assembled Nanowires on Semiconductor Surfaces. *J. Mater. Sci.* **2006**, *41*, 4568–4603.
7. Kubo, O.; Shingaya, Y.; Aono, M.; Nakayama, T. One-Dimensional Schottky Contact between ErSi₂ Nanowire and Si(001). *Appl. Phys. Lett.* **2006**, *88*, 233117.
8. Lee, S.; Shinde, A.; Ragan, R. Morphological Work Function Dependence of Rare-Earth Disilicide Metal Nanostructures. *Nanotechnology* **2009**, *20*, 035701.
9. Zeng, C.; Kent, P. R. C.; Kim, T.; Li, A.; Weitering, H. H. Charge-Order Fluctuations in One-Dimensional Silicides. *Nat. Mater.* **2008**, *7*, 539–542.
10. Jo, C.; Cao, J. X.; Shinde, A.; Ragan, R.; Wu, R. Q. First Principles Studies of Adsorption of Pd, Ag, Pt, and Au on Yttrium Disilicide Nanowires. *Chem. Phys. Lett.* **2008**, *454*, 327–331.
11. Ragan, R.; Kim, S.; Li, X.; Williams, R. S. Platinum Passivation of Self-Assembled Erbium Disilicide Nanowire Arrays on Si(001). *Appl. Phys. A: Mater. Sci. Process.* **2005**, *80*, 1339–1342.
12. You, J. P.; Choi, J. H.; Li, X.; Kim, S.; Williams, R. S.; Ragan, R. Regular Arrays of Monodisperse Platinum/Erbium Disilicide Core Shell Nanowires and Nanocrystals on Si(001) via a Self-assembled Template. *Nano Lett.* **2006**, *6*, 1858–1862.
13. Schuberta, M. M.; Hackenberga, S.; Veenb, A. C.; Muhlerb, M.; Plzakc, V.; Behm, R. J. CO Oxidation over Supported Gold Catalysts—“Inert” and “Active” Support Materials and Their Role for the Oxygen Supply during Reaction. *J. Catal.* **2001**, *197*, 113–122.
14. Daniel, M.; Astruc, M. Gold Nanoparticles: Assembly, Supramolecular Chemistry, Quantum-Size-Related Properties, and Applications toward Biology, Catalysis, and Nanotechnology. *Chem. Rev.* **2004**, *104*, 293–346.
15. Liu, Z. P.; Hu, P.; Alavi, A. Catalytic Role of Gold in Gold-Based Catalysts: A Density Functional Theory Study on the CO Oxidation on Gold. *J. Am. Chem. Soc.* **2002**, *124*, 14770–14779.
16. Chen, Y.; Crawford, P.; Hu, P. Recent Advances in Understanding CO Oxidation on Gold Nanoparticles using Density Functional Theory. *Catal. Lett.* **2007**, *119*, 21–28.
17. Liu, B. Z.; Nogami, J. A Scanning Tunneling Microscopy Study of Dysprosium Silicide Nanowire Growth on Si(001). *J. Appl. Phys.* **2003**, *93*, 593–599.
18. Yang, J. S.; Cai, Q.; Wang, X. D.; Koch, R. Morphological Evolution of Erbium Disilicide Nanowires on Si(001). *Surf. Interface Anal.* **2004**, *36*, 104–108.
19. Shinde, A.; Wu, R. Q.; Ragan, R. Thermodynamic Driving Forces Governing Assembly of Disilicide Nanowires. *Surf. Sci.* **2010**, *604*, 1481–1486.
20. Si atoms diffuse to the Si(001) surface and hence each of them should contribute about a ~ 5.4 eV to the total

- energy since original surface Si atoms are covered and converted to bulk-like atoms during this process.
21. Beierlein, T. A.; Brutting, W.; Riel, H.; Haskal, E. I.; Muller, P.; Riess, W. Kelvin Probe Investigations of Metal Work Functions and Correlation to Device Performance of Organic Light-emitting Devices. *Synth. Met.* **2000**, *111*, 295–297.
 22. Abukawa, T.; Enta, Y.; Kashiwakura, T.; Suzuki, S.; Kono, S.; Sakamoto, T. Photoemission Study of the Negative Electron Affinity Surfaces of O/Cs/Si(001) 2×1 and O/K/Si(001) 2×1 . *J. Vac. Sci. Technol., A* **1990**, *8*, 3205–3209.
 23. Hammer, B.; Norskov, J. K. Theoretical Surface Science and Catalysis—Calculations and Concepts. *Adv. Catal.* **2000**, *45*, 71–129.
 24. Baschuk, J. J.; Li, X. G. Carbon Monoxide Poisoning of Proton Exchange Membrane Fuel Cells. *Int. J. Energy Res.* **2001**, *25*, 695–713.
 25. Chen, M. S.; Kumar, D.; Yi, C. W.; Goodman, D. W. The Promotional Effect of Gold in Catalysis by Palladium-Gold. *Science* **2005**, *310*, 291–293.
 26. Bader, R. F. W. Atoms in Molecules. *Acc. Chem. Res.* **1985**, *18*, 9–15.
 27. Kresse, G.; Furthmüller, J. Efficient Iterative Schemes for *ab initio* Total-Energy Calculations using a Plane-Wave Basis Set. *Phys. Rev. B: Condens. Matter Mater. Phys.* **1996**, *54*, 11169–11186.
 28. Wang, Y.; Perdew, J. P. Correlation Hole of the Spin-Polarized Electron Gas, with Exact Small-Wave-Vector and High-Density Scaling. *Phys. Rev. B: Condens. Matter Mater. Phys.* **1991**, *44*, 13298–13307.
 29. Kresse, G.; Joubert, J. From Ultrasoft Pseudopotentials to the Projector Augmented-Wave Method. *Phys. Rev. B: Condens. Matter Mater. Phys.* **1999**, *59*, 1758–1775.
 30. Magaud, L.; Veuillen, J. Y.; Lollman, D.; Nguyen Tan, T. A.; Papaconstantopoulos, D. A.; Mehl, M. J. Electronic Structure of ErSi₂ and YSi₂. *Phys. Rev. B: Condens. Matter Mater. Phys.* **1992**, *46*, 1299–1304.
 31. Rogero, C.; Koitzsch, C.; González, M. E.; Aebi, P.; Cerdá, J.; Martín-Gago, J. A. Electronic Structure and Fermi Surface of Two-Dimensional Rare-Earth Silicides Epitaxially Grown on Si(111). *Phys. Rev. B: Condens. Matter Mater. Phys.* **2004**, *69*, 045312–045321.
 32. Woffinden, C.; Eames, C.; Menard, H.; Tear, S. P.; Pratt, A. Surface Electronic Structure of Two- and Three-Dimensional Holmium Silicide on Si(111). *Phys. Rev. B: Condens. Matter Mater. Phys.* **2009**, *79*, 245406.
 33. Shinde, A.; Cao, J. X.; Ouyang, W. J.; Wu, R. Q.; Ragan, R. Determination of Preferential Rare Earth Adatom Adsorption Geometries on Si(001). *Phys. Lett. A* **2009**, *373*, 3459–3463.
 34. Shinde, A.; Cao, J. X.; Lee, S.; Wu, R. Q.; Ragan, R. An Atomistic View of Structural and Electronic Properties of Rare Earth Ensembles on Si(0 0 1) Substrates. *Chem. Phys. Lett.* **2008**, *466*, 159–164.